JOURNAL OF THEORETICAL
AND APPLIED MECHANICS
64, 3, pp. 257–273, Warsaw 2026
https://doi.org/10.15632/jtam-pl/226326

FATIGUE DAMAGE PROCESS INVESTIGATION OF 18NI300 STEEL SPECIMENS MANUFACTURED BY LPBF METHOD

Roland PAWLICZEK, Cyprian SKÓRA*

Opole University of Technology, Faculty of Mechanical Engineering, Opole, Poland
*corresponding author, *c.skora@student.po.edu.pl*

The fatigue response of additively manufactured maraging steel MS1 produced by laser powder bed fusion (LPBF) was experimentally investigated. Uniaxial tension-compression fatigue tests were conducted at cycle asymmetry ratios $R = -1$, -0.5, and 0 to assess the influence of mean stress on fatigue life. The results demonstrated a pronounced effect of the stress ratio on fatigue performance. Two-step loading sequences – low-high (Lo-Hi) and high-low (Hi-Lo) – were applied to examine damage accumulation under non-constant loading conditions. A load asymmetry sensitivity factor was determined and the applicability of classical fatigue damage models was evaluated.

Keywords: maraging steel 18Ni300; additive manufacturing; fatigue life; stress ratio R.

1. Introduction

The additive manufacturing (AM) is a process based on the successive joining layer-by-layer of the material without the need for additional tooling or machining operations. Among AM techniques, selective laser melting (SLM) is one of the most widely used methods for metallic materials. In SLM, metal powder is selectively melted by a high-power laser according to CAD-generated cross sections, enabling the production of complex geometries with applications in aerospace, automotive, medical and defense industries (Croccolo *et al.*, 2018). Compared with conventional subtractive manufacturing, AM shortens supply chains, reduces material waste and allows greater design flexibility. However, the process is also associated with high energy consumption and challenges in controlling material properties and dimensional tolerances (Frazier, 2014; Afkhami *et al.*, 2019). Current literature on AM materials mainly focuses on the influence of process parameters, build orientation and post-processing treatments on mechanical properties (Croccolo *et al.*, 2018).

In industrial applications, maraging steel 300 (18Ni300, MS1) has attracted considerable attention due to its high strength, good ductility, weldability, and excellent fatigue resistance. MS1 is a low-carbon Fe-Ni martensitic steel strengthened by precipitation hardening. Owing to its very low carbon content, the alloy exhibits good machinability and weldability making it suitable for AM technologies and tooling, aerospace, marine, military, and automotive engineering applications. Despite its promising properties, the fatigue behaviour of additively manufactured MS1 steel still requires further investigation (Raju & Rosen, 2021; Cyr *et al.*, 2018; Solberg *et al.*, 2021).

A number of studies on 18Ni300 have demonstrated that the fatigue performance of AM maraging steel strongly depends on post-processing and manufacturing conditions. Cyr *et al.* (2018) showed significant anisotropy of mechanical properties caused by build orientation, while Rigon *et al.* (2018) reported that specimens built at 0° exhibited fatigue strengths that were 45 % to 60 % higher than those oriented at 90°. Similar anisotropic behaviour and lower fatigue strength compared with conventionally manufactured materials were observed by Damon *et al.* (2019). In contrast, Meneghetti *et al.* (2017) found no significant influence of orientation on tensile properties or fatigue behaviour in both as-built and aged conditions. Solberg *et al.* (2021) demonstrated that specimens fabricated closer to vertical orientation achieved longer fatigue life than horizontally oriented built samples. Similar work by Cerezo *et al.* (2024) showed that build orientation and defect morphology significantly affected crack propagation behaviour, with larger pores promoting faster crack growth.

Other studies also emphasized the importance of post-processing operations. Croccolo *et al.* (2018) reported that machining combined with heat treatment significantly improved fatigue strength, whereas heat treatment alone had little effect. Raju and Rosen (2021) similarly observed that aging treatment improved fatigue life, although machining produced the greatest enhancements. Yang *et al.* (2026) reported that solution-aging treatment improved mechanical properties through precipitation strengthening and microstructural refinement, while dos Santos Silva *et al.* (2026) demonstrated a substantial increase in tensile strength after heat treatment, accompanied by reduced ductility. Zhao *et al.* (2024) compared additively manufactured and cast material of 18Ni300 maraging steel and observed superior strength and plasticity of AM specimens due to their refined microstructure. The influence of processing parameters was also highlighted by Jose and Mishra (2026), who observed improved fatigue life for specimens produced using a stripe scanning strategy and further enhancements after heat treatment.

Investigations by Branco *et al.* (2021) and Karolczuk *et al.* (2024) indicated that surface and subsurface defects, particularly unmelted regions generated during the AM process, play a dominant role in crack initiation and fatigue damage. Under variable-amplitude loading, Marciniak *et al.* (2024) observed cyclic softening and identified surface and near-surface defects as the primary crack initiation sites. Investigation by Macek *et al.* (2024) linked fatigue life to fracture-surface topography and demonstrated that incorporating roughness parameters improved fatigue-life predictions. Karolczuk and Kurek (2025) reported that mean stress and surface topography play a significant role in fatigue damage accumulation and life prediction.

Just as research into the influence of the structure of additively manufactured materials on their strength is important, understanding the material response under various loading conditions is equally important. It is crucial for industries utilizing these modern manufacturing techniques to obtain information on the validation of the methods and algorithms used to design structural components with regard to additively manufactured materials. Do damage accumulation processes in such materials follow the mechanisms known from conventionally manufactured materials?

Although numerous investigations have addressed the effects of build orientation, heat treatment, manufacturing parameters and defect characteristics on the fatigue behaviour of LPBF-manufactured 18Ni300 maraging steel, the available literature remains focused primarily on constant-amplitude fatigue under a single stress ratio ($R = -1$). To the best of the authors' knowledge, systematic S-N characteristics covering different cycle asymmetry ratios for the as-built state of specimens are not available. Moreover, studies investigating the combined influence of the mean stress, cycle asymmetry and variable-amplitude block loading on the fatigue behaviour of LPBF-manufactured 18Ni300 are scarce. In particular, experimental verification of fatigue damage accumulation under low-high (Lo-Hi) and high-low (Hi-Lo) loading sequences, together with the evaluation of mean stress sensitivity and the applicability of commonly used mean stress correction models, has not yet been comprehensively reported for the examined material.

Therefore, the present study provides a comprehensive experimental investigation of the fatigue behaviour of LPBF-manufactured 18Ni300 maraging steel under different cycle asymmetry ratios ($R = -1$, -0.5, and 0). Firstly, preliminary constant-amplitude fatigue tests were performed to establish complete S-N characteristics for each loading condition. Based on these results, the material sensitivity factor to cycle asymmetry was determined and the applicability of the Smith–Watson–Topper (SWT) mean stress correction model was evaluated. Furthermore, two-stage Lo-Hi and Hi-Lo block-loading experiments were carried out to investigate fatigue damage accumulation under variable-amplitude loading. The analysis was complemented by tensile tests and hysteresis loop measurements, providing additional insight into the cycle deformation behaviour of the material. The obtained results provide an experimental dataset that is currently unavailable or insufficient in the literature for the fatigue behaviour of LPBF-manufactured 18Ni300 maraging steel in the as-built condition under different cycle asymmetry ratios and block-loading sequences. The study contributes to a better understanding of mean stress effects and fatigue damage accumulation.

2. Mean stress and calculation models

Programmed fatigue tests enable the reproduction of service loading conditions of structures and devices under laboratory conditions by applying selected cyclic loads. Loading histories may include variable amplitudes and mean stress values defined by the cycle asymmetry ratio R. Mean stress is an important factor affecting fatigue behaviour. It influences the maximum permissible stress amplitude. In engineering structures, mean stress often results from self-weight or operational tasks such as material transport and therefore should be considered in fatigue analyses (Pawliczek, 2005; Chiou & Yip, 2003). To evaluate fatigue life of 18Ni300 under different stress ratios, Solberg *et al.* (2021) investigated the influence of build orientation on the fatigue performance on LPBF-manufactured 18Ni300 maraging steel, fabricated in ten different orientations (from 0° to 135° in 15° increments). Specimens were aged at 500 °C for 5 h before removal from the build platform. All specimen surfaces were machined except for one surface that remained in the as-built condition. The authors performed fatigue tests under a stress ratio of $R = 0$ at a loading frequency of 30 Hz using a constant stress level of approximately 500 MPa, corresponding to a fatigue life of approximately $1 \cdot 10^5$ cycles. To enable comparison with fatigue data reported in the literature under fully reversed loading ($R = -1$), the authors applied the SWT mean stress correction model, which is as follows:

$$\sigma_{ar} = \sigma_{\max}\sqrt{\frac{1-R}{2}}, \tag{2.1}$$

where σ_{ar} is the stress amplitude at $R = -1$, and $\sigma_{\max}$ is the maximum stress during the load cycle at the given value of R.

The corrected fatigue data showed good agreement with the available results obtained under $R = -1$, thus confirming the applicability of the SWT approach for comparing fatigue performance under different stress ratios.

An important aspect of fatigue analysis is the assessment of the influence of the load sequence and stress level on damage accumulation. A commonly used approach is block-loading, usually divided into two stages with significantly different stress amplitudes. In two-step loading tests, referred to as Lo-Hi and Hi-Lo sequences, the material is first subjected to either low or high stress amplitudes and then loaded at the opposite level in the second stage. The first block is typically specified by the number of cycles n_1 at stress amplitude σ_1, while the second block is applied at stress amplitude σ_2 until failure. The presence of mean stress during such tests strongly affects damage accumulation and may lead to significant differences in fatigue life between applied sequences. Among available cumulative damage models, the Palmgren–Miner linear damage rule (LDR) was adopted due to its extensive use in fatigue engineering and its role as a reference model for evaluating sequence effects under variable loading conditions. Its application enables direct comparison between the experimentally observed damage accumulation and the predictions based on linear summation of fatigue damage. The linear damage rule is expressed as

$$D = \sum_{i=1}^{n} \frac{n_i}{N_i}, \tag{2.2}$$

where D is the degree of damage, n_i is the number of applied cycles at a given stress amplitude, N_i is the number of cycles to failure at the same stress amplitude.

According to this model, the total damage under ideal conditions should equal 1. However, under two-step loading, Lo-Hi sequences generally produce damage values greater than 1, whereas the Hi-Lo loading path results in damage values below 1 (Pawliczek, 2014; 2018).

In the present study, the classical, historically oldest model is used to generate the basic S-N curves (Murakami *et al.*, 2021). This model was employed by the same research group to describe MS1 material in studies (Croccolo *et al.*, 2018). Fatigue curves can be expressed using logarithmic or power functions, as in Eq. (2.3) or Eq. (2.4). The stress amplitude is determined as follows:

$$\log(N) = b + a \cdot \log(\sigma), \tag{2.3}$$

$$\sigma = 10^{b/a} \cdot N^{1/a}, \tag{2.4}$$

where N denotes the number of cycles, a and b are the equation parameters, and σ is the stress amplitude.

3. Material

Specimens for fatigue tests were manufactured using EOS MS1 maraging steel powder (European 1.2709), in accordance with the geometry shown in Fig. 1 and in compliance with the recommendations of the standard ASTM International (2021). The specimens were produced by the laser powder bed fusion (LPBF) process using the EOS M280 system in a nitrogen atmosphere. The specimens were built along the Z-axis on a platform preheated to 40 °C. Default process parameters for LPBF, supplied by EOS, were applied: laser beam power 285 W, scan speed 960 mm/s, layer thickness 40 μm and scan rotation 67°. The manufactured specimens were cleaned by micro-blasting using glass beads with a diameter of 90 μm to 150 μm at a low flow pressure of 300 kPa (Blast 2 Softline K1 device, FerroECOBlast) without any further machining. Figure 2 presents the tensile test curves obtained for two specimens. The force–elongation (F–ΔL) curve is linear, and after reaching the maximum value of load, there is a large increase in deformation with decreasing load. This indicates that the material has high elasticity. Mechanical parameters of 18Ni300 maraging steel are contained in Table 1. For the maximum force, the registered elongation was 0.588 mm. The axial stiffness of specimen is $k \approx 206$ kN/mm. Vickers hardness measurements yielded a mean value of 371 ±5 HV5. The measured hardness of the specimens is consistent with the range reported for additively manufactured 18Ni300 maraging steel in the as-built condition. The scatter of the results confirms good material homogeneity.

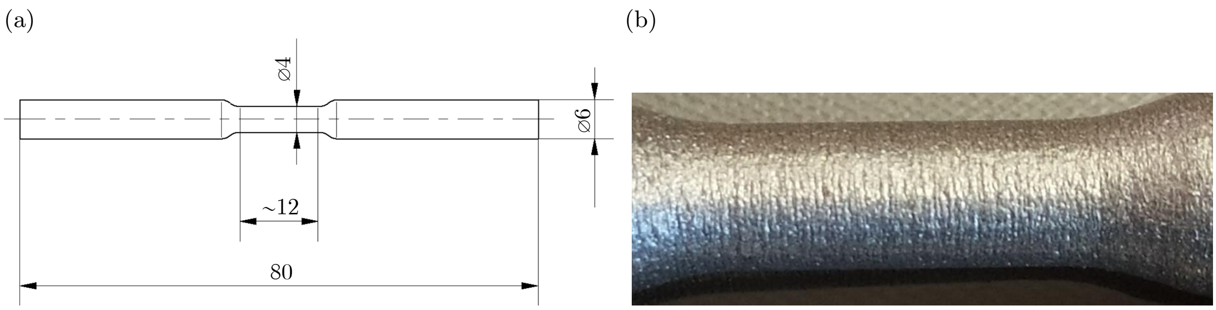

Fig. 1. (a) Specimen geometry; (b) view of the fusion line of successive layers.

In (Karolczuk *et al.*, 2024), fatigue tests were carried out using specimens produced from the same powder and manufactured using the same LPBF process. To determine the actual

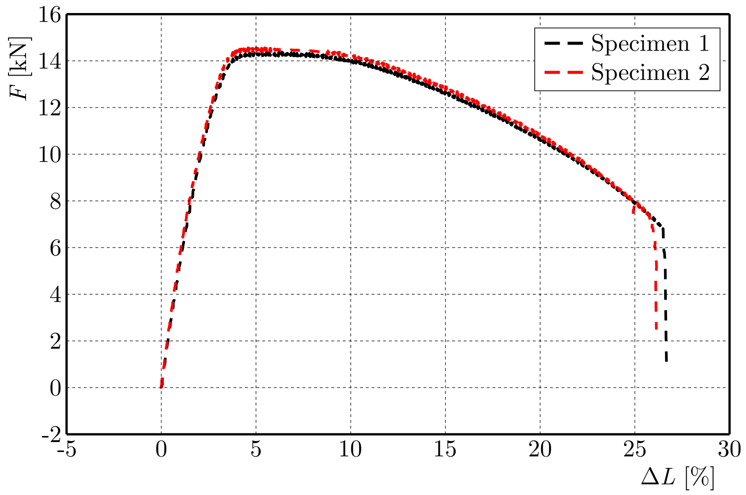

Fig. 2. Tensile test chart of MS1 material.

Table 1. Mechanical parameters of MS1.

Maximum force F_m [kN]	Young's modulus E [GPa]	Yield strength R_{p02} [MPa]	Ultimate strength R_m [MPa]	Elongation at fracture [%]
14.403	168	656.55	1205.70	26.67

chemical composition of the investigated material, the elemental contents were measured using an optical emission spectrometer (S3 MiniLab 300) on specimens aged at 490 °C. The reported values represent the mean of six measurements together with the corresponding 95 % confidence intervals and are presented in Table 2 alongside the nominal chemical composition provided by the powder supplier. The same study also includes images of the powder morphology and particle size distribution.

Table 2. Chemical composition of MS1 (wt.%) based on data reported by Karolczuk *et al.* (2024), according to information provided by supplier and from the measurements using an optical emission spectrometer.

	Ni	Mo	Co	Ti	Al	Cr	Si	Mn	C	Fe
Supplier	17–19	4.5–5.2	8.5–9.5	0.6–0.8	0.05–0.15	0–0.5	0–0.1	0–0.1	0–0.03	Balance
Spectrometer	17.6 ±0.2	5.4 ±0.0	8.7 ±0.2	0.6 ±0.0	0.07 ±0.01	0.05 ±0.02	0.09 ±0.01	0.2 ±0.0	0.01 ±0.0	Balance

The surface topography of the as-built specimens was characterized using a surface profilometer Alicona InfiniteFocus G4. After scanning the sample surface, the software generated a graph of the sample's topography and a roughness profile over a 4.5 mm measurement section. The program then divided the profile into 5 segments, each 0.8 µm long, where for each segment the distance between the maximum peak and the deepest valley was determined, and finally the arithmetic mean of these five segment measurements was calculated as the R_z parameter and arithmetic mean roughness R_a parameter, defined as the arithmetic mean deviation of the roughness profile from the mean value of the measurement section. The measured parameters were 19.21 µm and 3.40 µm, respectively. Representative surface topography and the corresponding roughness profile are presented in Fig. 3 and Fig. 4. The results confirm the relatively rough surface typical of LPBF-manufactured specimens in the as-built condition, which may promote stress concentration and facilitate fatigue crack initiation.

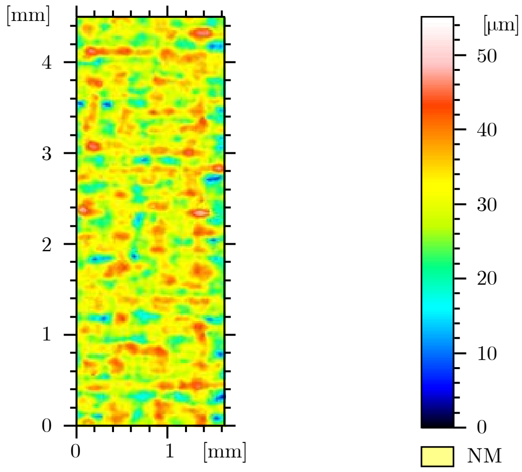

Fig. 3. Surface topography of the as-built specimen.

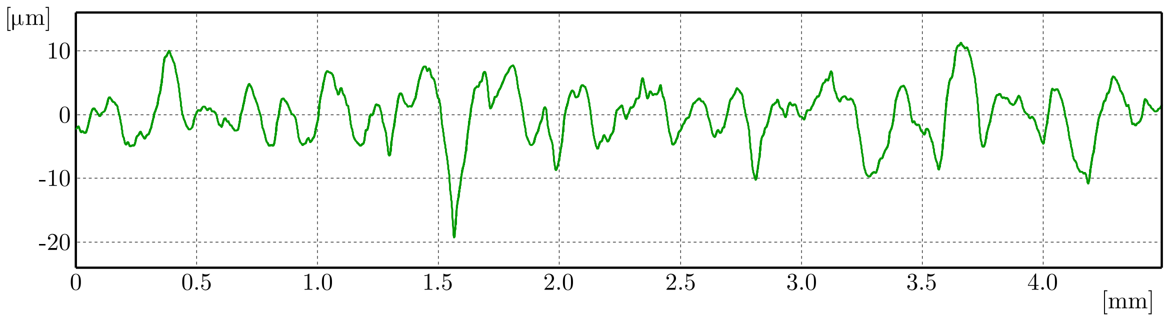

Fig. 4. Roughness profile (S-L) of as-built specimen of 18Ni300 maraging steel.

4. Methodology

For fatigue tests on specimens shown in Fig. 1, an Instron Electropuls E10000 testing system with a maximum load capacity of 10 kN was used, equipped with dedicated control software. Uniaxial tension-compression tests controlled by force/load at a frequency of ∼5 Hz were performed under sinusoidal loading with constant amplitude for the cycle asymmetry ratio $R = -1$, and under sinusoidal loading with constant amplitude including mean load values for $R = -0.5$ and $R = 0$. The load (force) during the test was applied as parallel to the build direction of samples. With changes in the R ratio according to Eqs. (4.1) and (4.2), the contribution of mean stress is as follows: $\sigma_m = 0$ for $R = -1$; $\sigma_m = 1/3\sigma_a$ for $R = -0.5$; $\sigma_m = \sigma_a$ for $R = 0$:

$$R = \frac{\sigma_{\text{min}}}{\sigma_{\text{max}}}, \tag{4.1}$$

$$\sigma_a = \frac{\sigma_{\text{max}} - \sigma_{\text{min}}}{2}, \qquad \sigma_m = \frac{\sigma_{\text{max}} + \sigma_{\text{min}}}{2}, \tag{4.2}$$

where σ_{max} is the maximum stress amplitude and σ_{min} is the minimal stress amplitude.

For low-cycle fatigue (LCF) tests, the selected ranges of stress amplitude σ_a for $R = -1$ were between 600 MPa and 1000 MPa. With an increase in the cycle asymmetry ratio to $R = -0.5$, the maximum stress range σ_{max} was 588 MPa to 718 MPa. For $R = 0$, σ_{max} was 538 MPa to 718 MPa. It should be noted that the maximum stresses described in this paper are defined as nominal values and are used solely to describe the loads. Results of the preliminary fatigue tests on LPBF-manufactured samples of 18Ni300 maraging steel, designed to determine S-N curves, are presented in Table 3.

Table 3. Results of the preliminary fatigue tests for different cycle asymmetry ratios.

Cycle asymmetry ratio	σ_a [MPa]	σ_m [MPa]	$\sigma_{\max}$ [MPa]	$N_{\exp}$ [cycle]
$R = -1$	600	–	600	18235
	650	–	650	10424
	675	–	675	9134
	700	–	700	5499
	800	–	800	4367
	900	–	900	2156
	1000	–	1000	376
$R = -0.5$	539	180	718	13324
	441	147	588	22041
	490	163	653	15271
	539	180	718	11291
	441	147	588	39187
	490	163	653	21139
$R = 0$	326	326	654	48592
	302	302	604	49197
	359	359	718	29060
	269	269	538	68442
	359	359	718	28012

Two-step block fatigue tests were also carried out using the Instron Electropuls E10000 testing system. The block loading tension-compression tests were force/load controlled at a frequency of ~5 Hz. The load ranges were selected based on the results of fatigue tests and the S-N curve equations shown in Fig. 7. Using the obtained equations, theoretical numbers of cycles to failure N were determined for specific stress amplitude values σ_a. Tests consisted of selecting appropriate loads for Hi-Lo and Lo-Hi experiments so that, in the first block (Hi- or Lo-), the specimen was subjected to tension-compression for a specified number of cycles, ranging from 20 % to 60 % of the theoretical fatigue life N_1 for the given stress amplitude σ_{a1}, with corresponding mean stress σ_{m1}. After completing the required number of cycles under the first block load, the stress amplitude and mean stress values were changed to those of the second block (σ_{a2}, σ_{m2}) corresponding to -Hi or -Lo. The tests were concluded when the specimen fractured or when the stiffness of the system was lost. Figure 5 presents the loading paths used in the experiments for different cycle asymmetry ratios. The approach for sequence tests is schematically presented in Fig. 6.

$R = -1$
Low block
$\sigma_a = 600$ [MPa]
$N = 14122$ [cycle]
High block
$\sigma_a = 675$ [MPa]
$N = 7640$ [cycle]

$R = -0.5$
Low block
$\sigma_a = 490$ [MPa]
$\sigma_m = 163$ [MPa]
$N = 18362$ [cycle]
High block
$\sigma_a = 539$ [MPa]
$\sigma_m = 179$ [MPa]
$N = 12118$ [cycle]

$R = 0$
Low block
$\sigma_a = 359$ [MPa]
$\sigma_m = 359$ [MPa]
$N = 30199$ [cycle]
High block
$\sigma_a = 384$ [MPa]
$\sigma_m = 384$ [MPa]
$N = 24785$ [cycle]

Fig. 5. Loading path for two-stage block sequences.

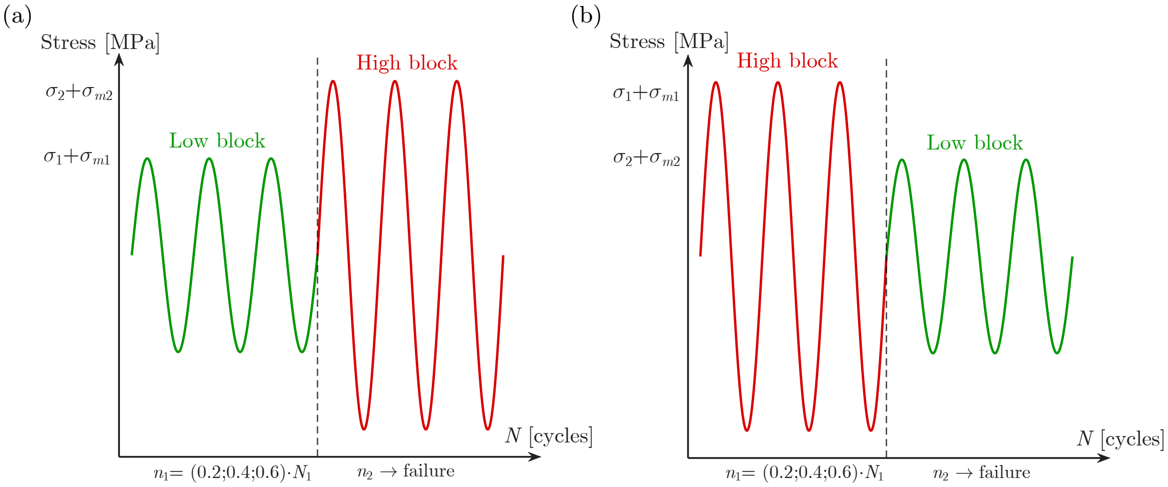

Fig. 6. Experimental campaign: (a) Lo-Hi sequence; (b) Hi-Lo sequence.

5. Fatigue characteristics

From the uniaxial tensile fatigue tests conducted in the LCF regime, the fatigue lives obtained for loads without mean stress are generally consistent with the experimental results reported in (Raju & Rosen, 2021; Rigon *et al.*, 2018; Branco *et al.*, 2021; Meneghetti *et al.*, 2019). For fatigue tests carried out under mean stress conditions, the results reported in the literature typically concern specimens tested at a cycle asymmetry ratio of $R = 0$. Additionally, the specimens used in these studies were subjected to further treatments, such as heat treatment in the form of aging at 490 °C (Solberg *et al.*, 2021; Frazier, 2014). On the other hand, fatigue tests for $R = -0.5$ are uncommon. Therefore, in both cases $R = 0$ and $R = -0.5$, for untreated material, there is no direct point of reference.

S-N curves and equations for different cycle asymmetry ratios in LCF are shown in Fig. 7. As can be observed, at higher stress amplitudes, the fatigue lives for $R = -1$ and $R = -0.5$ are similar, while for $R = 0$, the values are only slightly higher. As the stress amplitude decreases for $R = -1$, the number of cycles to failure also decreases, achieving the longest fatigue lives at the lowest amplitudes compared to the other curves. For $R = -0.5$, the number of cycles increases as the amplitude decreases, but to a lesser extent than for $R = -1$. The greatest differences occur

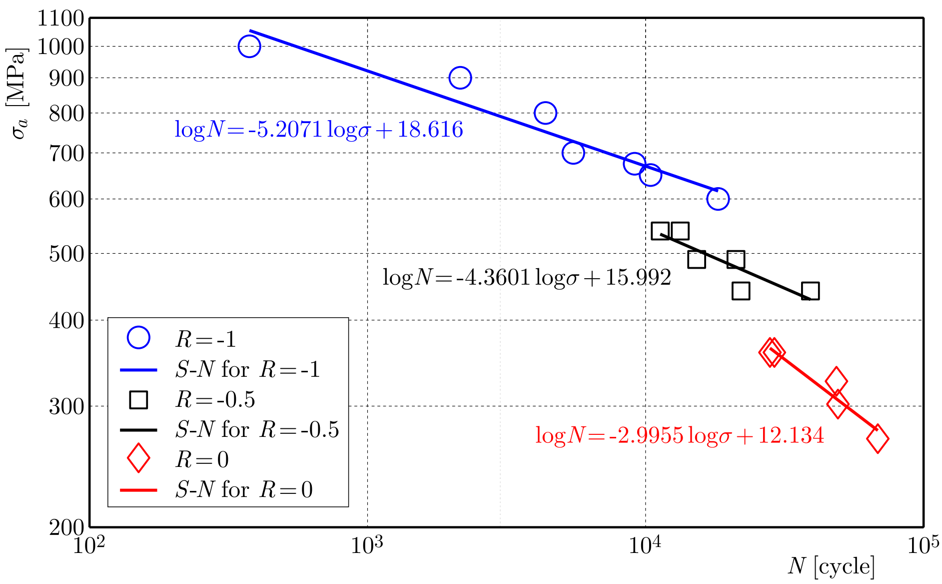

Fig. 7. *S-N* curves for additively manufactured MS1 maraging steel.

at $R = 0$. Up to about 800 Mpa to 900 MPa amplitude, the fatigue lives obtained at $R = 0$ are higher than those for $R = -0.5$ and $R = -1$. When the amplitude drops below this range, fatigue lives for $R = -1$ become higher than for $R = 0$, while those for $R = -0.5$ remain lower. Only at a stress amplitude of ∼600 MPa, the fatigue lives for $R = 0$ become lower than for $R = -0.5$. At the lowest stress amplitude, the fatigue lives for $R = 0$ are the smallest compared to the other two. In general, fatigue life increased with decreasing maximum stress amplitude. Among all tested conditions the lowest fatigue lives were recorded for fully reversed loading ($R = -1$). Introducing a positive mean stress component for $R = -0.5$, where $\sigma_m = \frac{1}{3}\sigma_a$, resulted in longer fatigue lives despite comparable stress amplitudes. The highest fatigue resistance was obtained for $R = 0$, indicating a strong influence of the stress ratio and mean stress on the fatigue performance of the material.

The hysteresis loops were determined on the actuator displacement recorded by the Instron Electropuls 10000 testing machine. From the hysteresis loops (Fig. 8) in the stress–displacement system, it should be noted that they are narrow, suggesting minor plastic deformations in the tested material or even an elastic state of deformations. It is also worth noting that at a large number of cycles (towards the end of fatigue life), a slight shift of the loop towards strain is observed, which may suggest the occurrence of creep phenomena. This effect is most evident in tests conducted at $R = 0$, and is caused by the presence of significant mean stress. In contrast, for tests without mean stress, the hysteresis loops for the three selected measurement points exhibited almost identical shapes, with only slight differences in the initial portions.

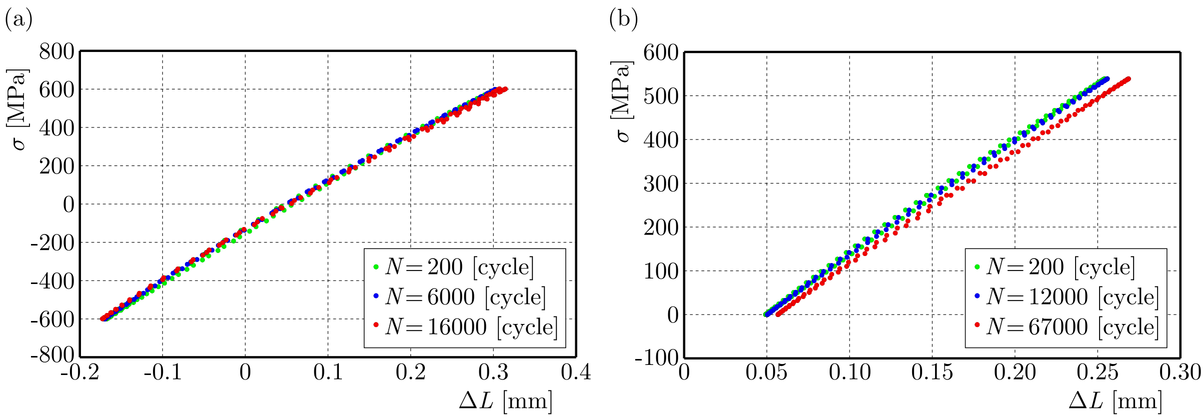

Fig. 8. Hysteresis loops: (a) $R = -1$, $\sigma_a = 600$ MPa; (b) $R = 0$, $\sigma_a = 269$ MPa.

6. Stress ratio factor approach

Gasiak and Pawliczek (2003) proposed a model for determining the material sensitivity factor to cycle asymmetry ψ, as a function of the number of cycles to failure, based on experimental fatigue test results. The proposed model is based on the Haigh diagram and on a simplified linear relationship between the stress amplitude σ_a and the mean stress σ_m. For the limiting amplitudes of stresses, the following expression is adopted:

$$\Delta\sigma = \Delta\sigma_{-1} - 2\psi_\sigma\sigma_m, \tag{6.1}$$

$$\psi_\sigma(N) = \frac{2\Delta\sigma_{-1}(N) - \sigma_0(N)}{\sigma_0(N)}, \tag{6.2}$$

where $\psi_\sigma(N)$ is the material sensitivity factor to cycle asymmetry for a given number of cycles to failure, $\Delta\sigma_{-1}(N)$ is the stress amplitude under cyclic bending/tension at the number of cycles to failure, $\sigma_0(N)$ is the maximum stress under pulsating cycles in bending/tension for a given number of cycles to failure.

To evaluate the effect of cycle asymmetry on changes in the S-N characteristics for different cycle asymmetry ratios (as presented in Fig. 7), three fatigue life ranges of $2\cdot10^4$, $4\cdot10^4$, $6\cdot10^4$ cycles to failure were selected. Using equations of S-N curves determined from experimental results, stress amplitude values were determined for these fatigue ranges. Figure 9 presents the results, together with equations of the curves for the given stress ratios. The calculated theoretical fatigue points largely overlap with the linear regression curves, and the equations of the curves shown in Fig. 9 are nearly identical to those presented in Fig. 7.

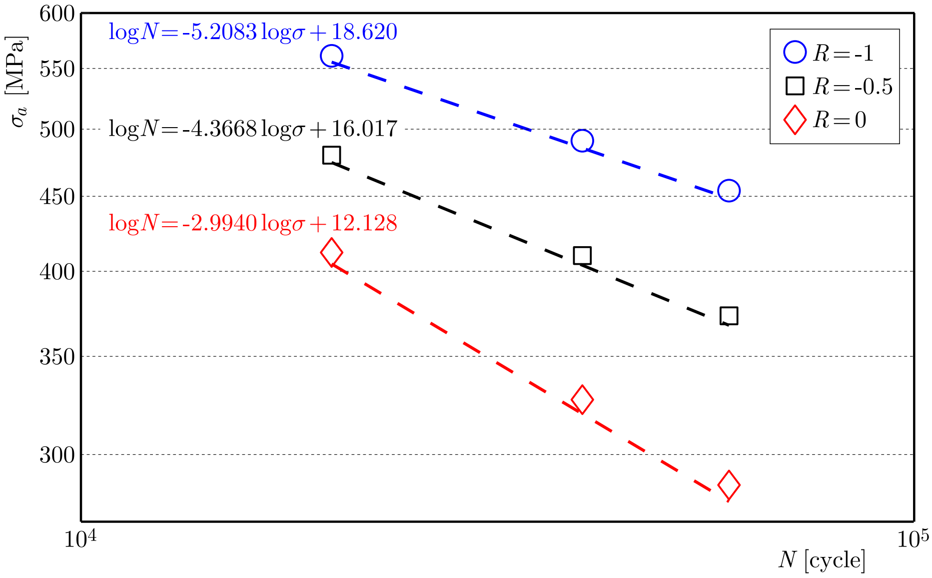

Fig. 9. Fatigue life N versus estimated stress amplitude for the assumed fatigue lives.

Figure 10 shows the relationship between the normalized mean stress (σ_m/R_m) and the normalized stress amplitude (σ_a/σ_{AT}), where σ_{AT} is a substitute amplitude value calculated based on the applied model, using previously determined points presented in Fig. 9. A comparison of the points corresponding to different values of the cycle asymmetry ratio R indicates that the SWT parameter (Eq. (2.1)) predicts slightly lower values of amplitudes compared to the

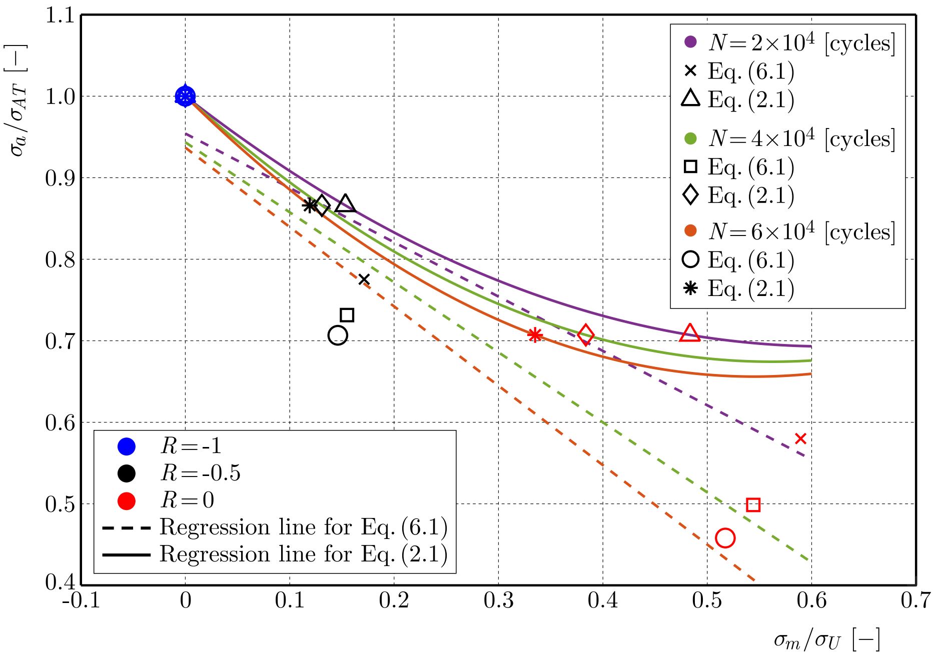

Fig. 10. Normalized Haigh diagram.

material sensitivity factor to cycle asymmetry ψ approach (Eq. (6.1)). The SWT parameter shows good correlation with the regression curves. Equation (6.1) is a linear model, and for cycle asymmetry ratios $R = -0.5$ and $R = -1$ shows weak correlation with the regression line. The best correlation is observed for the highest values of maximal stress amplitudes for $R = 0$. The differences between the SWT parameter (Eq. (2.1)) and the material sensitivity factor ψ (Eq. (6.1)) decrease with the contribution of mean stress amplitude.

Table 4 summarizes the comparison between the experimental values of the sensitivity factor to cycle asymmetry and those calculated using Eq. (6.2). As can be seen, the obtained values are very similar, especially for fatigue lives of $4 \cdot 10^4$ and $6 \cdot 10^4$. The most noticeable difference occurs at the smallest adopted number of cycles to failure, where the difference is about 3.5 %. However, this is still negligible, and therefore the formula used to determine the sensitivity factor to cycle asymmetry can be considered suitable for the investigated material.

Table 4. Comparison of experimental and calculated values of the material sensitivity factor.

N [cycles]	ψ_{exp}	ψ_{cal} (Eq. (6.2))	Relative error [%]
$2 \cdot 10^4$	0.350	0.362	3.43
$4 \cdot 10^4$	0.500	0.503	0.60
$6 \cdot 10^4$	0.590	0.592	0.34

7. Fatigue test results analysis

The fatigue test results of two-stage loading tests are presented in Fig. 11 to Fig. 13, where the lower part of the bar is equivalent to the first sequence with the given number of cycles and the upper bar is the second sequence of the test, which lasted until failure occurred. For the cycle asymmetry ratio $R = -1$, the predicted fatigue lives according to the S-N curve are $1.4 \cdot 10^4$ cycles for 600 MPa and $7.6 \cdot 10^3$ cycles for 675 MPa. In Lo-Hi tests, the second block n_2 for $n_1/N_1 = 20\,\%$ and $60\,\%$ were similar, reaching about 1.1 to $1.2 \cdot 10^4$ cycles. The greatest

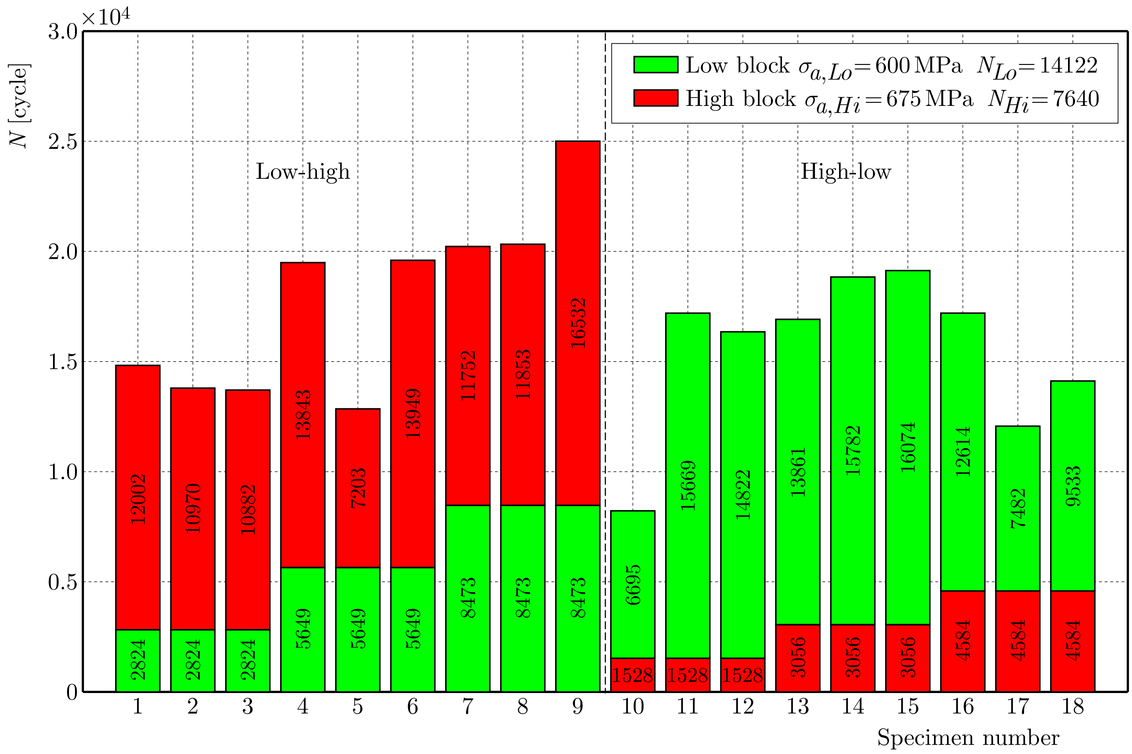

Fig. 11. Results of two-step fatigue tests for $R = -1$.

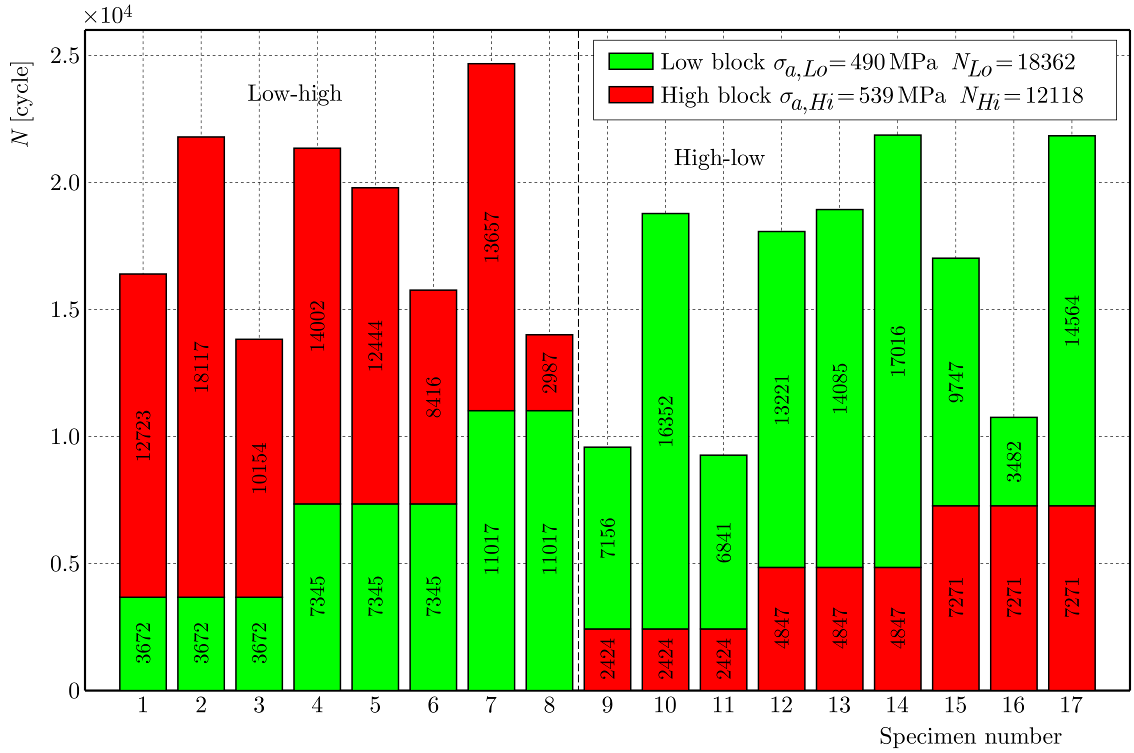

Fig. 12. Results of two-step fatigue tests for $R = -0.5$.

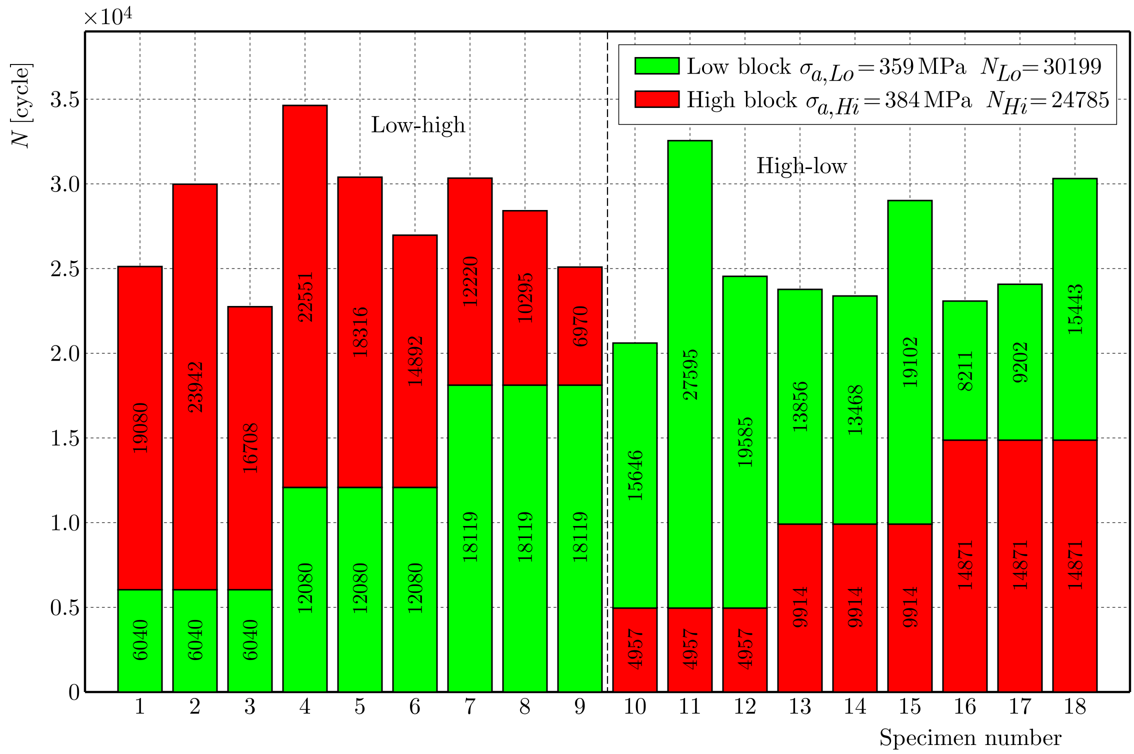

Fig. 13. Results of two-step fatigue tests for $R = 0$.

scatter of results occurred for $n_1/N_1 = 40\,\%$, where the lowest fatigue lives were recorded in this series. All specimens failed during tests. Therefore, the presented number of cycles corresponds to fatigue life at fracture. The figures directly represent the distribution of fracture lives for Lo-Hi and Hi-Lo loading sequences.

For the Hi-Lo loading path at $R = -1$, the highest fatigue lives were observed for $n_1/N_1 = 40\,\%$ while the lowest occurred for $60\,\%$. Considerable scatter between specimens was noted especially for the lowest and highest first-block shares. Mean results indicated a gradual decrease in fatigue life with increasing participation of the high-stress first block.

At the cycle asymmetry ratio $R = -0.5$ the applied maximum stresses were 653 MPa for the low sequence and 718 MPa for the high sequence with the contribution of mean stress of $\sigma_m = \frac{1}{3}\sigma_a$. Estimated fatigue lives from the corresponding equation from Fig. 7 are $1.8 \cdot 10^4$ cycles and $1.2 \cdot 10^4$ cycles. In this series of tests, substantial scatter was observed, particularly for every share of the first block. In some cases, the contribution of the second block differed by up to 4 times. The most consistent behaviour was observed for the 40 % share of the first block for Hi-Lo series, while the remaining loading paths exhibited larger variations in fatigue life.

The highest values of maximum stress amplitudes were applied during the final series for the cycle asymmetry ratio $R = 0$. Based on the S–N curve, the predicted maximum stress amplitude was 718 MPa for the low-sequence loading block and 767 MPa for the high-sequence loading block, corresponding to fatigue lives of 30 199 and 24 785 cycles, respectively. In the Lo-Hi tests, the highest fatigue life was obtained for the $n_1/N_1 = 40\,\%$, reaching approximately $3.46 \cdot 10^4$ cycles. The lowest scatter was observed for the intermediate loading ratio. In the Lo-Hi tests, the greatest durability of all experiments was observed when the first loading sequence accounted for $n_1/N_1 = 40\,\%$, with fatigue lives reaching up to $3.5 \cdot 10^4$ cycles. However, increasing the share of the first loading block resulted in lower repeatability and greater scatter. Overall, the results indicate that both the cycle asymmetry ratio R and the sequence of loading blocks significantly influence the fatigue response of additively manufactured samples of MS1 maraging steel. Considerable scatter in fatigue life, particularly under variable-amplitude loading, also confirms the strong sensitivity of the material to loading history and internal defects characteristic of the AM process.

Representative fracture surfaces obtained after the two-step block loading tests are presented in Fig. 14 and Fig. 15. Regardless of the loading sequence and the share of the first block, fatigue crack initiation was most frequently associated with manufacturing-related defects of the LPBF process. The dominant initiation sites were located either at the specimen surface or in the near-surface region, where stress concentration effects are the highest. The fractographic observations revealed several characteristic features: crack initiation region (1), rapid fracture regions (2), spherical gas pores (3), fatigue crack propagation zones with visible striations (4), lack-of-fusion (LoF) defects (5), and surface irregularities associated with the specimen contour (6). The presence of pores and LoF defects confirms that internal discontinuities remain

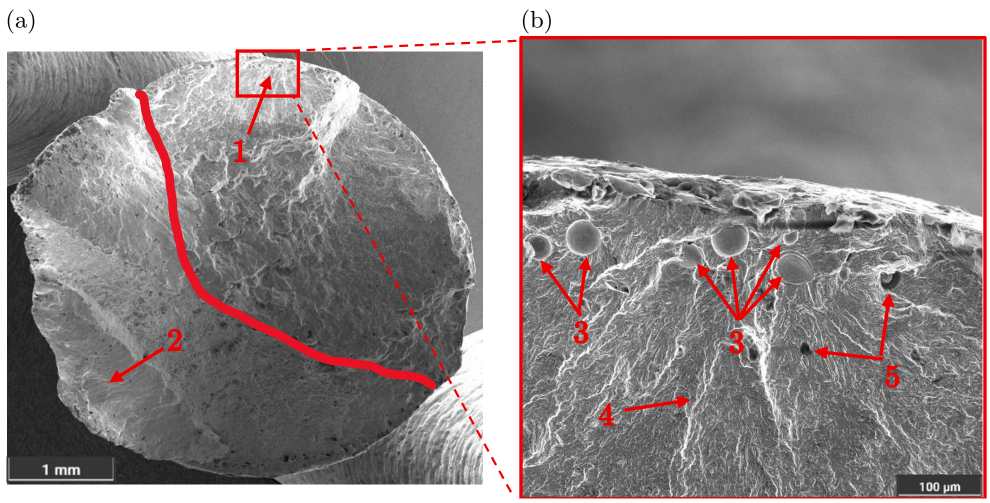

Fig. 14. Surface of the fracture in the specimen for Lo-Hi block tests, $R = -0.5$; $n_1/N_1 = 0.2$, at magnifications: (a) 100×; (b) 1000×.

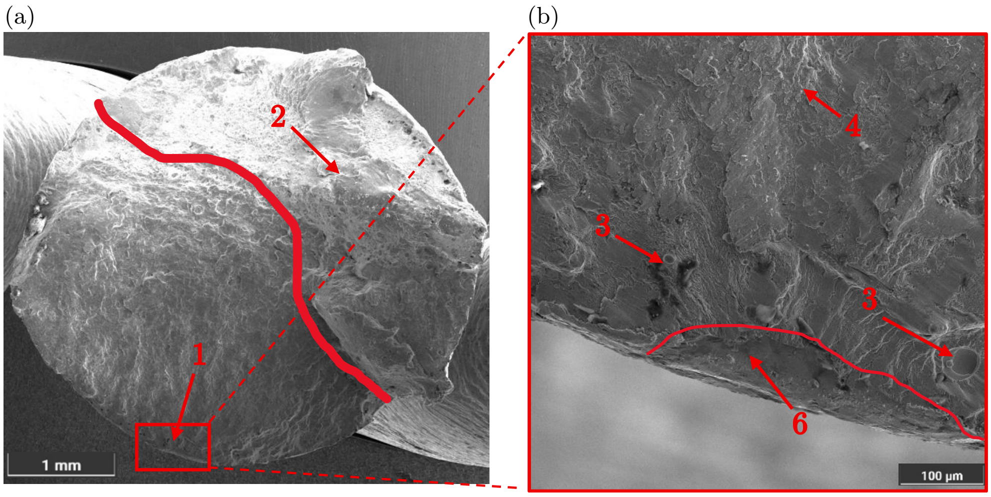

Fig. 15. Surface of the fracture in the specimen for Hi-Lo block tests, $R = -1$; $n_1/N_1 = 0.4$, at magnifications: (a) 100×; (b) 1000×.

the primary fatigue-critical features controlling crack nucleation in additively manufactured specimens.

8. Damage accumulation

Table 5 shows the mean damage accumulation results for the conducted fatigue tests. From the experimental results for the stress ratio $R = -1$, it can be observed that with an increasing

Table 5. Mean damage accumulation results for $R = -1$, $R = -0.5$, and $R = 0$.

Test	n_1/N_1	n_2/N_2	$D = n_1/N_1 + n_2/N_2$
$R = -1$			
Lo-Hi-20 %	0.20	1.107	1.307
Lo-Hi-40 %	0.40	0.787	1.187
Lo-Hi-60 %	0.60	0.642	1.242
Hi-Lo-20 %	0.20	0.770	0.970
Hi-Lo-40 %	0.40	0.863	1.263
Hi-Lo-60 %	0.60	0.375	0.975
$R = -0.5$			
Lo-Hi-20 %	0.20	1.128	1.328
Lo-Hi-40 %	0.40	0.959	1.359
Lo-Hi-60 %	0.60	0.687	1.287
Hi-Lo-20 %	0.20	0.551	0.751
Hi-Lo-40 %	0.40	0.805	1.205
Hi-Lo-60 %	0.60	0.505	1.105
$R = 0$			
Lo-Hi-20 %	0.20	0.803	1.003
Lo-Hi-40 %	0.40	0.750	1.150
Lo-Hi-60 %	0.60	0.397	0.997
Hi-Lo-20 %	0.20	0.693	0.893
Hi-Lo-40 %	0.40	0.512	0.912
Hi-Lo-60 %	0.60	0.363	0.963

share of the first block, the contribution of the second block to total damage decreases. An exception occurred in the Hi-Lo test with the first block at the 40 % of the predicted cycles to failure.

For the stress ratio $R = -0.5$, differences were also observed for both Lo-Hi and Hi-Lo sequences. In both cases, the contribution of the second block to total damage generally decreased with an increasing share of the first block. In the Lo-Hi test with a 60 % share of the first block, the smallest second-block contribution was observed in the series. Compared to the 20 % share, the damage value at 60 % was almost 65 % smaller, and compared to 40 %, it was 39 % smaller. Conversely, for the Hi-Lo sequence at the 40 % first-block share, the second-block damage contribution was the highest in the series: 32 % higher than at 20 %, and 37 % more than at 60 %.

For the stress ratio R = 0, the Lo-Hi tests showed similar second-block contributions for the 20 % and 40 % shares (difference <7 %). In contrast, the 60 % share was twice as small as second-block damage compared to the other two. For the Hi-Lo sequence, the contribution of the second block at the 20 % share was almost twice as high as observed for the 60 % share and 26 % higher compared with the 40 % share.

9. Conclusions

Fatigue testing is a crucial element in assessing performance potential of materials. The use of varied test methods, such as block loading, makes it possible to study material behaviour under variable loading conditions. Applying different stress ratios further expands the knowledge of possible applications of such materials under service conditions involving fluctuating loads and additional influencing factors. From the uniaxial tension-compression fatigue tests with different stress ratios and block sequences (Lo-Hi and Hi-Lo) on additively manufactured MS1 material, the following conclusions can be drawn:

- with a varying stress ratio and comparable stress amplitudes, the highest fatigue lives were observed for specimens tested with the mean stress present ($R = 0$), while the lowest fatigue lives were recorded for $R = -1$;
- with an increasing stress ratio, the stress amplitude values for $R = -0.5$ and $R = 0$ were lower than for $R = -1$; however, the maximum stress, which also includes mean stress, resulted in overall higher loading for $R = -0.5$ and $R = 0$ than for $R = -1$;
- S-N curves obtained for different stress ratios showed interesting behaviour, especially for $R = 0$, at lower amplitudes, fatigue life was higher than for the other ratios, while at maximum amplitudes the opposite was true, with the shortest lives observed;
- the material sensitivity factor to the stress ratio changed linearly with cycles to failure. The model effectively captured this behaviour;
- the second-block damage ratio n_2/N_2 generally decreased with increasing the first-block share n_1/N_1, with some exceptions;
- the Palmgren–Miner model fit best to sequential tests at $R = -1$. For Lo-Hi, the damage accumulation results matched the model assumptions, while for Hi-Lo at some test results the accumulation matched the Lo-Hi case. For the other Hi-Lo tests, the results aligned with the LDR model. At $R = -0.5$, deviations were observed at $n_1/N_1 = 0.4$, Hi-Lo showed higher accumulation compared to unity and at $R = 0$, Lo-Hi showed lower damage accumulation in comparison with other cycle asymmetry ratios;
- the greatest differences in damage accumulation were observed in the mean results: at $R = 0$ for Lo-Hi tests with $n_1/N_1 = 20\,\%$ and 60 %, less damage was generated, while for $R = -0.5$ in Hi-Lo tests with $n_1/N_1 = 40\,\%$ and 60 %, more damage was accumulated, in contradiction to the Palmgren–Miner model assumptions.

References

1. Afkhami, S., Dabiri, M., Alavi, S.H., Björk, T., & Salminen, A. (2019). Fatigue characteristics of steels manufactured by selective laser melting. *International Journal of Fatigue*, *122*, 72–83. https://doi.org/10.1016/j.ijfatigue.2018.12.029

2. ASTM International. (2021). *E466-21, Standard Practice for Conducting Force Controlled Constant Amplitude Axial Fatigue Tests of Metallic Materials*. ASTM International. https://doi.org/10.1520/E0466-21

3. Branco, R., Costa, J.D., Martins Ferreira, J.A., Capela, C., Antunes, F.V., & Macek, W. (2021). Multiaxial fatigue behaviour of maraging steel produced by selective laser melting. *Materials & Design, 201*, Article 109469. https://doi.org/10.1016/j.matdes.2021.109469

4. Cerezo, P.M., Cruces, A.S., Moore, S., Wheatley, G., & Lopez-Crespo, P. (2024). Characterisation of 18Ni300 steel CT specimens in a fatigue test manufactured by selective laser melting at 0°, 45° and 90°. *Theoretical and Applied Fracture Mechanics*, *134* (Part B), Article 104730. https://doi.org/10.1016/j.tafmec.2024.104730

5. Croccolo, D., De Agostinis, M., Fini, S., Olmi, G., Robusto, F., Ćirić Kostić, S., Vranić, A., & Bogojević, N. (2018). Fatigue response of as-built DMLS maraging steel and effects of aging, machining, and peening treatments. *Metals*, *8* (7), Article 505. https://doi.org/10.3390/met8070505

6. Cyr, E., Lloyd, A., & Mohammadi, M. (2018). Tension-compression asymmetry of additively manufactured maraging steel. *Journal of Manufacturing Processes*, *35*, 289–294. https://doi.org/10.1016/j.jmapro.2018.08.015

7. Damon, J., Hanemann, T., Dietrich, S., Graf, G., Lang, K.-H., & Schulze, V. (2019). Orientation dependent fatigue performance and mechanisms of selective laser melted maraging steel X3NiCoMoTi18-9-5. *International Journal of Fatigue*, *127*, 395–402. https://doi.org/10.1016/j.ijfatigue.2019.06.025

8. dos Santos Silva, B.C., Seixas, L.F., Callegari, B., Batalha, R.L., Reis, L., dos Santos Paula, A., Godefroid, L.B., Batalha, G.F., & Coelho, R.S. (2026). Influence of build orientation and thermal treatment on the fracture toughness of LPBF-manufactured 18Ni300 maraging steel. *Journal of Materials Research and Technology*, *40*, 577–592. https://doi.org/10.1016/j.jmrt.2025.12.134

9. Frazier, W.E. (2014). Metal additive manufacturing: A review. *Journal of Materials Engineering and Performance*, *23* (6), 1917–1928. https://doi.org/10.1007/s11665-014-0958-z

10. Gasiak, G., & Pawliczek, R. (2003). Application of an energy model for fatigue life prediction of construction steels under bending, torsion and synchronous bending and torsion. *International Journal of Fatigue*, *25* (12), 1339–1346. https://doi.org/10.1016/S0142-1123(03)00055-0

11. Jose, S.S.S., & Mishra, S.K. (2026). Effect of scanning strategies on low cycle fatigue and corrosion behaviour of LPBF 18Ni300 steel. *Materials Chemistry and Physics*, *362*, Article 132761. https://doi.org/10.1016/j.matchemphys.2026.132761

12. Karolczuk, A., & Kurek, A. (2025). Machine learning insight into the mean stress impact on fatigue life of additively manufactured 18Ni300 maraging steel under various multiaxial stress paths. *International Journal of Fatigue*, *198*, Article 109023. https://doi.org/10.1016/j.ijfatigue.2025.109023

13. Karolczuk, A., Kurek, A., Böhm, M., Derda, S., Prażmowski, M., Kluger, K., Żak, K., Pejkowski, Ł., & Seyda, J. (2024). Heterogeneous effect of aging temperature on the fatigue life of additively manufactured thin-walled 18Ni300 maraging steel tubular specimen. *Materials & Design*, *237*, Article 112561. https://doi.org/10.1016/j.matdes.2023.112561

14. Macek, W., Marciniak, Z., Lesiuk, G., Podulka, P., & Jiang, C.-P. (2024). The Smith–Watson–Topper parameter and fracture surface topography relationship for additively manufactured 18Ni300 steel subjected to uniaxial variable-amplitude loading. *Theoretical and Applied Fracture Mechanics*, *133* (Part B), Article 104607. https://doi.org/10.1016/j.tafmec.2024.104607

15. Marciniak, Z., Branco, R., Macek, W., Dobrzyński, M., & Malça, C. (2024). Cyclic deformation and fracture behaviour of additive manufactured maraging steel under variable-amplitude loading. *Theoretical and Applied Fracture Mechanics*, *129*, Article 104207. https://doi.org/10.1016/j.tafmec.2023.104207

16. Meneghetti, G., Rigon, D., Cozzi, D., Waldhauser, W., & Dabalà, M. (2017). Influence of build orientation on static and axial fatigue properties of maraging steel specimens produced by additive manufacturing. *Procedia Structural Integrity*, *7*, 149–157. https://doi.org/10.1016/j.prostr.2017.11.072

17. Meneghetti, G., Rigon, D., & Gennari, C. (2019). An analysis of defects influence on axial fatigue strength of maraging steel specimens produced by additive manufacturing. *International Journal of Fatigue*, *118*, 54–64. https://doi.org/10.1016/j.ijfatigue.2018.08.034

18. Murakami, Y., Takagi, T., Wada, K., & Matsunaga, H. (2021). Essential structure of *S-N* curve: Prediction of fatigue life and fatigue limit of defective materials and nature of scatter. *International Journal of Fatigue*, *146*, Article 106138. https://doi.org/10.1016/j.ijfatigue.2020.106138

19. Pawliczek, R. (2005). Fatigue life of specimens made of 18G2A steel under bending block loading for given values of mean load (in Polish). *Zeszyty Naukowe / Politechnika Opolska*, *83*, 167-174.

20. Pawliczek, R. (2014). Influence of the mean load value in fatigue block loading on strains. *Key Engineering Materials*, *598*, 195–200. https://doi.org/10.4028/www.scientific.net/KEM.598.195

21. Pawliczek, R. (2018). Evaluation of fatigue damage degree for specimens made of S355J0 steel subjected to bending block loads with mean load value. In D. Skibicki (Ed.), *Fatigue Failure and Fracture Mechanics XXVII: Proceedings of the XXVII Polish National Conference on Fatigue Failure and Fracture Mechanics*, *2028*(1), Article 020015. https://doi.org/10.1063/1.5066405

22. Raju, N., & Rosen, D.W. (2021). Fatigue properties of 3D printed maraging steel. In *Proceedings of the 32nd Annual International Solid Freeform Fabrication Symposium – An Additive Manufacturing Conference*, 831–841.

23. Rigon, D., Meneghetti, G., Görtler, M., Cozzi, D., Waldhauser, W., & Dabalà, M. (2018). Influence of defects on axial fatigue strength of maraging steel specimens produced by additive manufacturing. *MATEC Web of Conferences*, *165*, Article 02005. https://doi.org/10.1051/matecconf/201816502005

24. Solberg, K., Hovig, E.W., Sørby, K., & Berto, F. (2021). Directional fatigue behaviour of maraging steel grade 300 produced by laser powder bed fusion. *International Journal of Fatigue*, *149*, Article 106229. https://doi.org/10.1016/j.ijfatigue.2021.106229

25. Yang, T., Zeng, H., Liu, Z., Chen, P., Yang, C., Qiu, C., & Chu, P.K. (2026). Synergistic improvement of strength and elongation in laser-melting-deposited 18Ni300/316 heterostructured dual-phase steel by heat treatment. *Smart Materials in Manufacturing*, *4*, Article 100124. https://doi.org/10.1016/j.smmf.2026.100124

26. Zhao, M., Shen, S., Wang, H., Niu, L., Shi, J., Chen, Z., Wang, X., & Lu, B. (2024). Effect of heat treatment on microstructure and hydrogen embrittlement of additively manufactured and cast 18Ni300 maraging steel. *Journal of Materials Research and Technology*, *33*, 9566–9579. https://doi.org/10.1016/j.jmrt.2024.12.002

Manuscript received May 20, 2026; accepted for publication July 23, 2026;
published online September 7, 2026.